Cellulose
https://doi.org/10.1007/s10570-025-06385-2

ORIGINAL RESEARCH

Pd nanocatalyst supported on chitosan–waste oil microspheres for efficient degradation of industrial pollutants in water

Kaan Karaoğlu · Nuray Yılmaz Baran · Zehra Özçifçi · Hakkı Türker Akçay · Talat Baran

Received: 29 August 2024 / Accepted: 11 January 2025

Abstract Disposal of industrial pollutants is one of the most important working topics today. Pd–doped catalysts have high efficiency in the degradation of many organic pollutants. Within the scope of this study, waste engine oil (WEO) was used as activated carbon (AC) source and then AC was encapsulated with chitosan (CS) to prepared chitosan–based microbeads (CS/WEO AC) for catalyst support. After treatment with glyoxal as cross–linker, Pd nanoparticles with spherical shape and 16.8 nm diameter were decorated on the microbeads (Pd@CS/WEO AC). Efficiency of Pd@CS/WEO AC on the reduction of 4-nitrophenol (4-NP), 4-nitro-o-phenylenediamine (4-NPDA), 2-nitroaniline (2-NA), 4-nitroaniline (4-NA) as nitroarens; methylene blue (MB), methyl orange (MO), and rhodamine B (RhB) as organic dyes; Cr(VI) and $K_3[Fe(CN)_6]$ was examined in aqueous media. Developed Pd@CS/WEO AC nanocatalyst reduced nitroarenes, organic dyes, Cr(VI) and $K_3[Fe(CN)6]$ in very short times (0–130 s). Based on kinetic studies, the rate constants for Pd@CS/WEO AC–catalyzed reduction reactions of 2–NA, 4–NP, 4–NA, 4–NPDA, MO, RhB, $[Fe(CN)_6]^{3-}$, and Cr(VI) were found to be 0.018 s^{-1}, 0.007 s^{-1}, 0.026 s^{-1}, 0.012 s^{-1}, 0.021 s^{-1}, 0.065 s^{-1}, 0.048 s^{-1}, and 0.042 s^{-1}, respectively. Additionally, it was confirmed that Pd@CS/WEO AC is a long–lasting catalyst, as it was reused for five successive runs in the reduction of 4–NP. In this study, we aim to design new materials by modifying carbon–containing waste sources with biological macromolecules and investigate the possible applications of these materials to remove some pollutants from water sources.

Keywords Waste engine oil · Chitosan · Microbeads · Hybrid catalyst

Supplementary Information The online version contains supplementary material available at https://doi.org/10.1007/s10570-025-06385-2.

K. Karaoğlu (✉)
Department of Chemistry and Chemical Processing Technologies, Vocational School of Technical Sciences, Recep Tayyip Erdoğan University, 53020 Rize, Turkey
e-mail: kaan.karaoglu@erdogan.edu.tr

N. Yılmaz Baran
Department of Chemistry Technology, Vocational School of Technical Sciences, Aksaray University, 68100 Aksaray, Turkey

Z. Özçifçi · H. T. Akçay
Department of Chemistry, Faculty of Arts and Sciences, Recep Tayyip Erdoğan University, 53020 Rize, Turkey

T. Baran
Department of Chemistry, Faculty of Science and Letters, Aksaray University, 68100 Aksaray, Turkey

Introduction

Lubrication oils are chemicals with long–carbon chains which are produced from crude oil and used to prevent moving parts of machinery from friction

Published online: 29 January 2025

and wear. Some additives, such as viscosity index improvers, extreme pressure additives, and pour point depressants, are added to satisfy market demand (Widodo et al. 2020). Although lubricating oil is one of the main components that ensure stable engine operation in the automotive industry, waste engine oil obtained after periodic maintenance is a pollutant, and contains toxic components such as heavy metals, organometallics, and dithiophosphates, which limits recycling applications (Maceiras et al. 2017). Waste engine oil with an estimated annual production of 24 million metric tons could be considered a carbon source to design a carbon–based catalyst; in this way, the environmental risks can be reduced (Arpa et al. 2010; Suriani et al. 2015; Lam et al. 2015).

According to the United Nations (UN) UN–Water Integrated Monitoring Initiative for SDG 6, approximately 1.7 billion people have suffered from contaminated drinking water in 2021. UN also aims to minimize the industrial release of hazardous chemicals into water sources by 2030 (United Nation (UN-Water) 2021). Dyes, one of the most intensely produced synthetic organic chemicals, is a class of compounds that may be toxic for aquatic environments (Tkaczyk et al. 2020). At first glance, with more than 2.8×10^5 tons of discharged wastewater, textile industry seems to be the main source of this type of pollutants (Zhao et al. 2022). Additionally, the energy demand for wastewater treatment limits global carbon footprint reduction efforts for a sustainable environment (Luo et al. 2024). Therefore, designing effective wastewater treatment systems with low energy demand has attracted great attention from research groups to mitigate global warming. To this aim, some sophisticated catalysts were designed for decolorization of dyes by using solar energy (Khan et al. 2016). Carbon–based solid supports doped with transition metals could be promising green catalysts because of their easy production processes, high efficiency, and reusability to reach sustainable development for the water sanitation goal. Some efficient graphene–based heterogenous catalysts with mono– and bi–metallic transition metals have been fabricated to reduce nitroarens in aqueus media (Huang et al. 2023; Zhao et al. 2024; Hu et al. 2024).

Due to their high stability, non-toxicity, biocompatibility, and biodegradability, biopolymers are recognized as ideal catalyst support materials (Taya and Agarwal 2024). Chitosan (CS), one of the most important members of the biopolymer family, is produced by deacetylation of chitin (Jiménez-Gómez and Cecilia 2020). In addition to being inexpensive and environmentally friendly, CS can easily form complexes with different metals due to the free $–NH_2$ and –OH functional groups on its polymer chain (Liu et al. 2024a). These functional groups also allow for easy chemical modifications, enabling CS to be transformed into various forms such as hydrogel beads, films, composite, and gels (Sargin 2019; Zheng et al. 2020). Hydrogel beads obtained using a cross–linking agent are among the most important forms, especially in catalyst systems, because they allow for the easy recovery of the catalyst from the reaction medium. Therefore, CS can be combined with various organic/inorganic structures to form composites, and different metal nanoparticles can be deposited on this form to design new heterogeneous catalyst systems.

While making life easier with immense industrial processes, the innovative technologies may contribute environmental problems such as rapid depletion of natural resources, clean water supply, global warming, and waste management (Ullah et al. 2023). To contribute goals of sustainable environment, this work aims to prepare Pd/chitosan–based microbeads as a new heterogenous catalyst from WEO. To date, besides production of diesel–like fuel by pyrolysis reaction (Ramanathan and Santhoshkumar 2019), literature has mainly focused on refining (Widodo et al. 2020), purification (Fedosov et al. 2022), recycling (Hamawand et al. 2013), and rejuvenating properties of used engine oils (Al-Saffar et al. 2021). While WEO can be used as a sustainable carbon source in production of supercapacitor electrodes (Kaipannan et al. 2020), and carbon dots (K et al. 2022), to the best of our knowledge, this is the first proposal to use WEO as a carbon source in the design of a hybrid catalyst for catalytic reduction of organic dyes, nitroarenes, chromium (VI), and $K_3[Fe(CN)_6]$ in textile wastewater.

Experimental

Material and methods

WEO was supplied from a local car service. All chemicals were reagent grade and purchased from Sigma–Aldrich. The solutions were prepared with

ultra-pure water by using Human Corporation Zeneer Power 1 water purification system.

Synthesis of activated carbon (WEO AC)s

In the pre–carbonization step, 125 g of WEO was loaded in a beaker and 40 g of concentrated sulfuric acid was added with continuous stirring at room temperature. Then a watch glass was placed on beaker which was then heated to 180 ± 5 °C for 90 min. 50 g of partly solidified product was transferred into a ceramic boat, and then, under N_2 atmosphere, the boat was heated up to 600 °C with at a heating rate of 20 °C/min. At this point, the chamber was subjected to steam at a rate of 1 cm^3/min for 30 min while continuously heating up to 700 °C for 1 h. Then, the furnace was cooled down to room temperature, and obtained 3.53 ± 1.03 g of carbonized product was transferred to a desiccator.

Synthesis of CS/WEO AC hydrogel beads

2 g of prepared WEO AC were added to a chitosan (CS) solution (2% w:w, 100 mL of acetic acid) and stirred for 3 h. The CS/WEO AC mixture was then transferred into a burette and dropped into solution of water:NaOH:ethanol (40 mL:12 g:60 mL) to form CS/WEO AC hydrogel beads. The resulting CS/WEO AC hydrogel beads were collected and washed with water several times. Finally, the CS/WEO AC hydrogel beads were cross–linked by refluxing with glyoxal (5 mL) in 70 mL of ethanol media. The cross-linked CS/WEO AC hydrogel beads were collected from the reaction media, rinsed with ethanol, and dried at room temperature.

Fabrication of Pd@CS/WEO AC hydrogel beads

The loading of Pd nano–particles (Pd NPs) on the surface of the CS/WEO AC hydrogel beads was performed by stirring 0.15 g of $PdCl_2$ and 1.0 g of CS/WEO AC hydrogel beads into 50 mL of ethanol for 5 h at 70 °C. Pd@CS/WEO AC hydrogel beads were filtered, washed with ethanol and dried to apply as heterogenous nanocatalyst against reduction of persistent environmental pollutants.

Characterization of Pd@CS/WEO AC hydrogel beads

The X-ray diffractometry (XRD) spectra were recorded in Rigaku Smartlab system. Scanning electron microscope (SEM) images of the samples were recorded by a JEOL JSM 6610, and the elemental composition of the samples was measured using an energy dispersive X-ray spectrometer, Oxford Instruments Inca X–act, combined with SEM. The Transmission Electron Microscope (TEM) images of samples were recorded by Hitachi HT-7700 equipped with the Lanthanum hexaboride electron beam gun with 40–120 eV. Surface properties were studied by BET analyzer (Quantachrome, USA) by nitrogen adsorption at −196 °C. The degassed of sample was performed under vacuum at 105 °C for fifteen hours before the measurement. The surface characteristics was calculated by Brunauer–Emmett–Teller (BET) and BJH (Barrett, Joyner, and Halenda), QSDFT (Quenched solid density functional theory) methods (Brunauer et al. 1938; Barrett et al. 1951; Neimark et al. 2009).

General procedure for the catalytic tests

Reduction of nitroarenes catalyzed by the Pd@CS/WEO AC hydrogel beads

1 mL of nitroarene (1×10^{-4} M) and 0.5 mL of an aqueous solution of $NaBH_4$ (0.05 M) were transferred into a quartz cuvette and stirred for 2 min. To initiate the reduction, Pd@CS/WEO AC hydrogel beads were then added to the reaction media, and stirred until reaction was completed. UV–Vis spectra were recorded at regular intervals to monitor the reduction process. After the reduction process of nitroarenes, Pd@CS/WEO AC hydrogel beads were separated from the media, washed with water, and dried to check its reusability performance.

Reduction of MB, MO, and RhB catalyzed by the Pd@CS/WEO AC hydrogel beads

1 mL of the solution of dye (methy orange: MO, rhodamine B: RhB, and methylene blue: MB at 0.1×10^{-5} M) and 0.5 mL of $NaBH_4$ solution (0.05 M) were combined in a quartz cuvette. Then, 5 mg of Pd@CS/WEO AC hydrogel beads was introduced

into the reaction medium, and the reduction was monitored with UV–visible spectroscopy and stirred until reaction was completed. After finishing of test, the recovery and reuse potential of the Pd@CS/WEO AC hydrogel beads were investigated by using the same procedure as above.

Reduction of the $K_3[Fe(CN)_6]$

1 mL of $K_3[Fe(CN)_6]$ solution (0.002 M), 0.5 mL of $NaBH_4$ solution (0.05 M), and 5 mg of Pd@CS/WEO AC hydrogel beads were placed into a quartz cuvette and stirred at room temperature. The reaction progress was checked with UV–visible spectroscopy by monitoring the changes in the absorbance band of $K_3[Fe(CN)_6]$ at 418 nm. Finally, Pd@CS/WEO AC hydrogel beads were recovered, washed, and dried using the same procedure as above.

Reduction of the Cr(VI)

The stock solution of Cr(VI) with a concentration of 3.4×10^{-4} M was prepared using $K_2Cr_2O_7$, and HCOOH was used as the reducing agent in the catalytic reduction experiment. 1 mL of $K_2Cr_2O_7$, 0.2 mL of HCOOH, and 5 mg of Pd@CS/WEO AC hydrogel beads were mixed and stirred at 50 °C and the reaction progress of the reduction of Cr(VI) to Cr(III) was monitored with UV–Vis analyses.

Results and discussion

Synthesis

First, carbonization process of the WEO was investigated at 600 °C under nitrogen atmosphere followed by activation step. Four types of activating agents, namely, alkaline (K_2CO_3, NaOH, and K_2SiO_3), acidic (H_3PO_4, HNO_3, and $H_4P_2O_7$), neutral ($ZnCl_2$, $FeCl_3$, and $NaNH_2$), and self–activating agents can be used to improve the specific surface area or pore volume of AC. These activation agents have some such disadvantages as corrosion on the equipment, waste of washing water, and unavoidable secondary pollution (Gao et al. 2020). Besides to reduce environmental risk as low as possible, we used steam activation for its low cost and efficiency (Mopoung and Dejang 2021). Then activated carbon was mixed with chitosan solution, and mixture reacted with glyoxal to obtain cross–linked hydrogel beads. Finally, Pd(0) was decorated on the surface of hydrogel beads (Scheme 1).

Structural characterization

The porosity characteristics of the obtained product (AC) was studied by BET method. The specific surface area and total pore volume of AC was calculated as 615.4 $m^2\ g^{-1}$ and 0.62 $cm^3\ g^{-1}$, respectively. The average pore diameter of AC was calculated size 4 nm. Mesopore volume was calculated as 0.4 $cm^3\ g^{-1}$ (65%) with BJH method. As can be seen in Fig. 1, AC showed type II isotherm with H4 type hysteresis according to IUPAC classification. In the AC isotherm, the sharp bend in the low–pressure region indicates microporosity resulting from monolayer adsorption. The equilibrium state in the range of 0.35–0.5 P/P_0 indicates that monolayer adsorption is completed, and multilayer adsorption has started. The unlimited increase in multilayer adsorption at $P/P_0=1$ suggests the presence of macropores in the structure. H4 hysteresis indicates capillary condensation in the presence of narrow–necked pores and can be seen in micro–mesoporous activated carbons (Thommes et al. 2015; Wang and Yu 2017). The pore size distribution of AC calculated by QSDFT method confirms the micro– and meso–porous structure, predominantly meso pores (Fig. 1). The specific surface area of Pd@CS/WEO AC was measured as 5 $m^2\ g^{-1}$ by single-point calculation using the BET method.

XRD patterns of CS/WEO AC and Pd@CS/WEO AC were recorded X–ray Diffractometer at 2θ from 5° to 90° (Fig. 2). In the XRD pattern of CS/WEO AC, which consists of a mixture of mineral oil–based activated carbon and chitosan, the bands observed at 2θ = 9.76° (020) and 20.08° (110) belong to semicrystalline chitosan, and the peak observed at 2θ = 34.62° (311) belongs to Fe_3O_4 (Han et al. 2014; Hao et al. 2021). While the peaks of chitosan in the XRD pattern of Pd@CS/WEO AC remained unchanged, the diffraction peaks observed at 2θ = 40.02°, 46.5°, 68.1°, 82.2° and 86.07 match indexed reflections to the (111), (200), (220), (311) and (222) diffraction planes of face-centered cubic (fcc) lattice of Pd (JCPDS = 46–1043). The disappearance of the Fe_3O_4 peak in Pd@CS/WEO AC indicates that Fe_3O_4 is

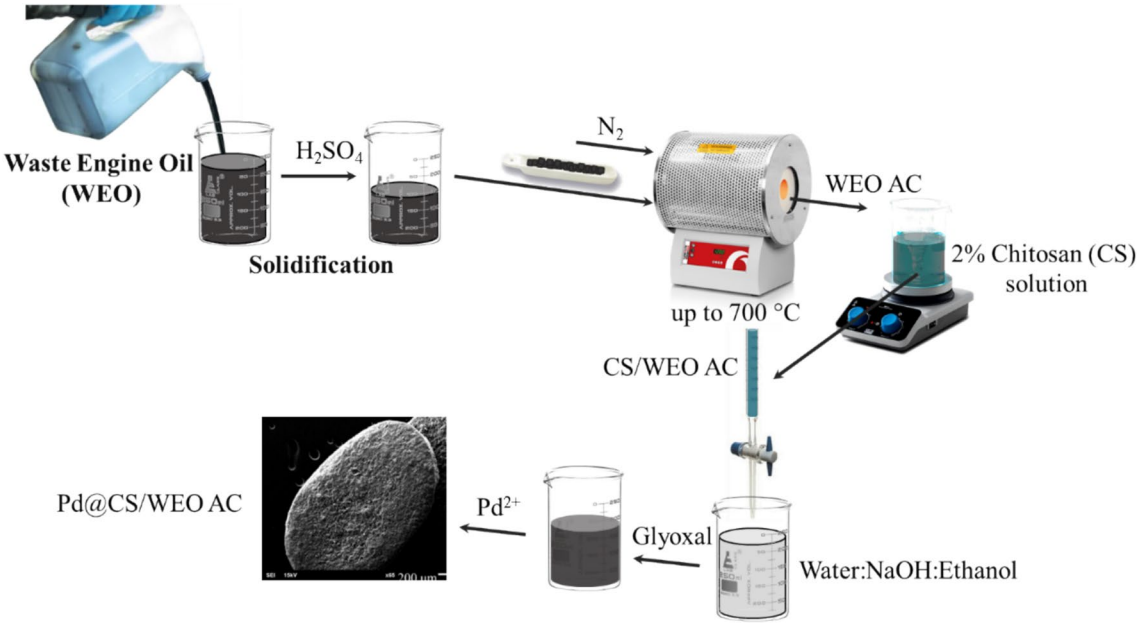

Scheme 1 Synthesis scheme of Pd@CS/WEO AC microbeads

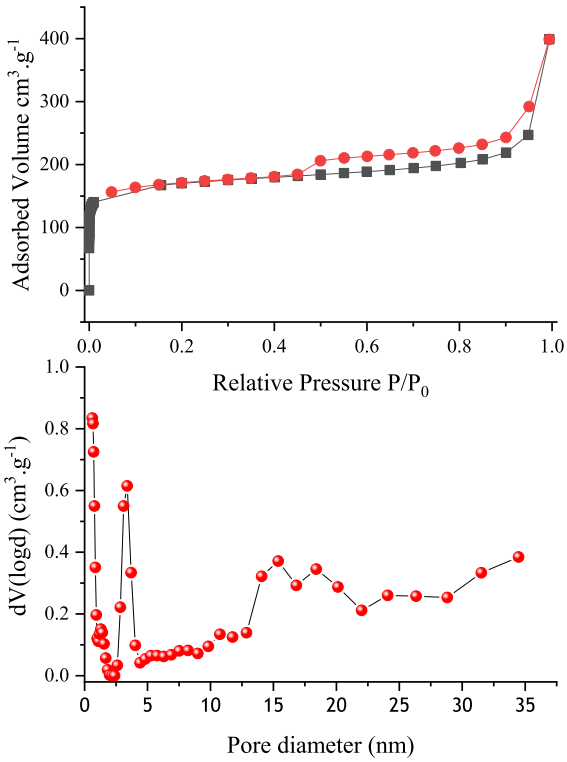

Fig. 1 BET isotherm and the pore size distribution of AC

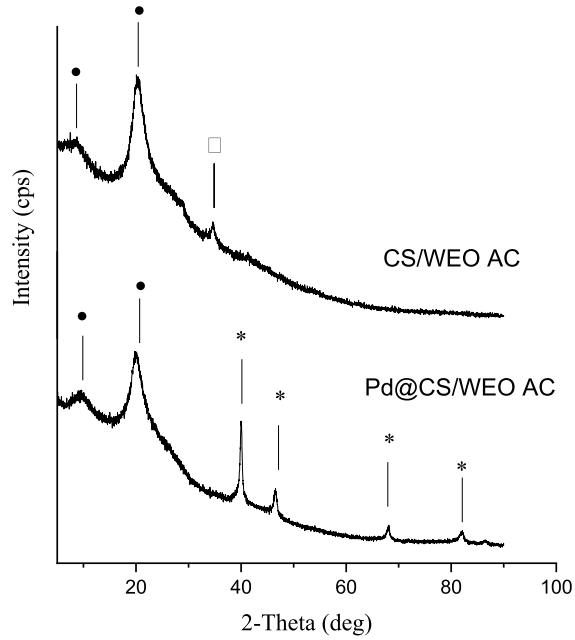

Fig. 2 XRD patterns of CS/WEO AC (top) and Pd@CS/WEO AC (bottom)

removed from the structure during Pd(0) catalyst preparation.

SEM images and EDS results of the Pd@CS/WEO AC sample are presented in Fig. 3. Figure 3a shows that the catalyst produced as a chitosan composite forms flat spherical forms as expected in the production method. As seen in Fig. 3b, when the material's surface is examined more closely, it is seen that cracks are spread throughout the material. EDS results of the Pd@CS/WEO AC sample showed that there was 14.9% Pd in the examined region of the structure. In addition, it was observed that the structure of the sample contained carbon, nitrogen and oxygen, as expected (Fig. 3c and d).

TEM images of Pd@CS/WEO AC hydrogel beads were recorded by Hitachi HT-7700 and given in Fig. 4. It seen from Fig. 4 that Pd–nanoparticles have been successfully decorated on the surface of the CS/WEO AC solid support. The size of the particle crystalline structures of Pd(0) nanoparticles was determined by using the Scherrer Eq. (1) with the X–ray line expansion method (Scherrer 1918; Wyckoff 1963).

$$D = \frac{k\lambda}{\beta_D cos\theta} \tag{1}$$

where D is the particle size in nanometers, λ is the wavelength of the incident X–ray (1.54056 A). For CuKα radiation, k is a constant which equals to 0.94, β is the peak width at half maximum intensity and θ is the peak position. The sharp peaks observed in the

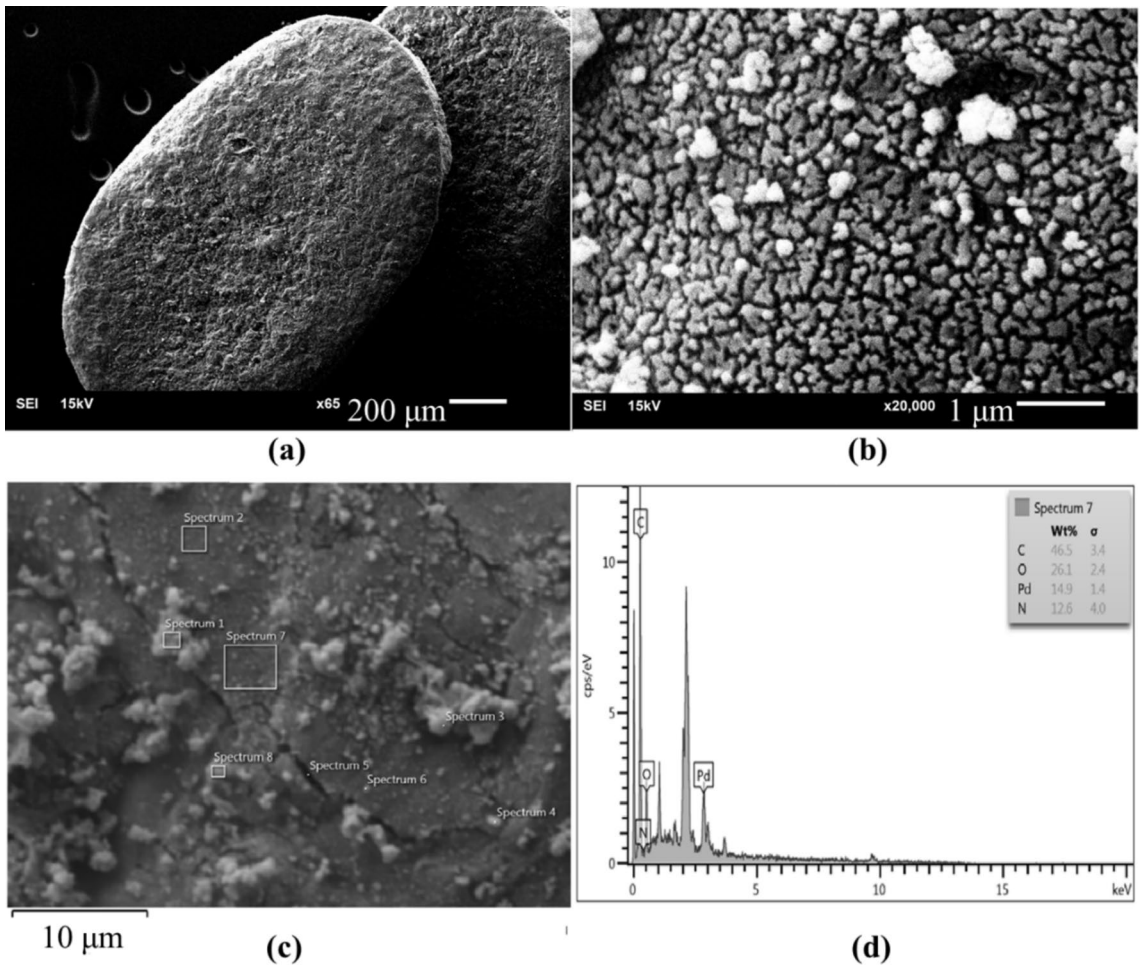

Fig. 3 SEM and EDS images of Pd@CS/WEO AC

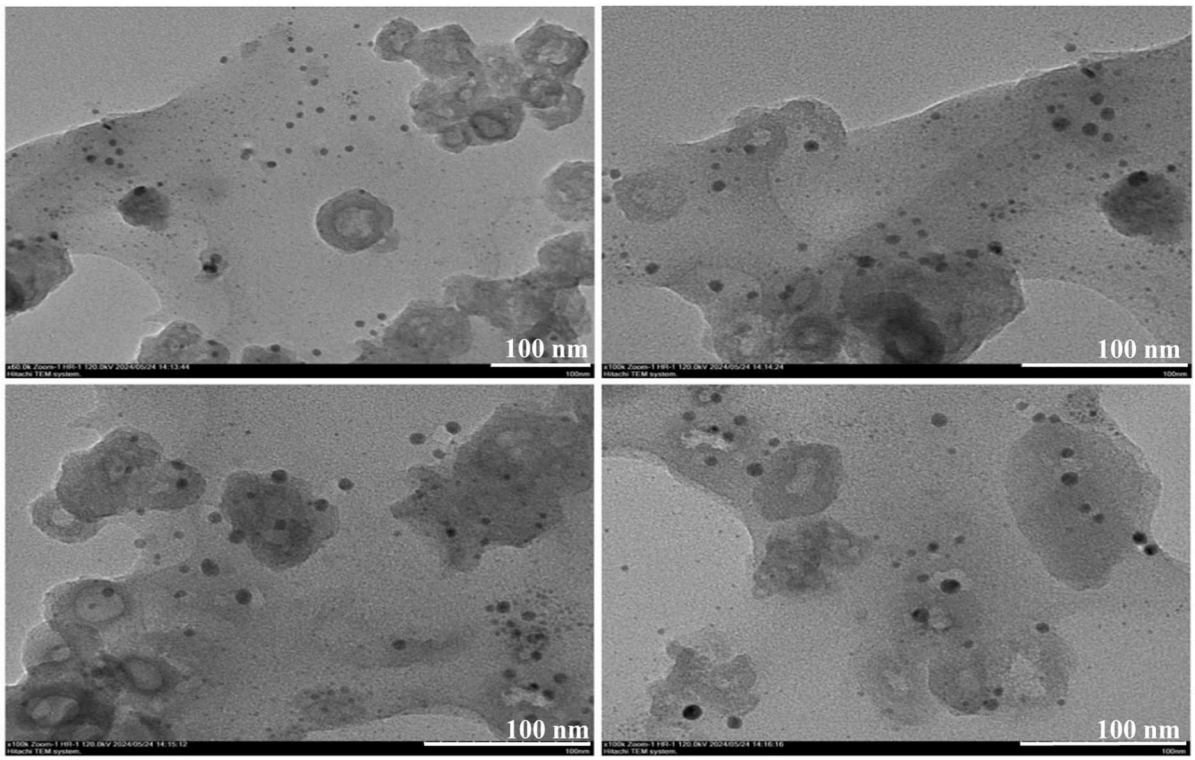

Fig. 4 TEM images of Pd@CS/WEO AC hydrogel beads

XRD pattern of Pd(0) indicate that the material has a nanocrystalline structure. According to the XRD patterns of the produced material, no mass residue and impurity was found. The data of the most intense peak observed at $2\theta = 40.02$ degree on the XRD pattern was used while calculating the microcrystalline size of Pd(0). The crystalline size of Pd(0) in the material was calculated as 16.8 nm by the Scherrer equation (Scherrer 1918).

Catalytic activity evaluation of Pd@CS/WEO AC hydrogel beads

The progress of the reductions of 2–nitroaniline (2–NA), 4–nitroaniline (4–NA), 4–nitrophenol (4–NP), and 4–nitro–o–phenylenediamine (4–NPDA) was studied using UV–vis spectrophotometer. The changes in the intensity of characteristic peaks were monitored at 414 nm for 2–NA, 402 nm for 4–NP, for 385 nm for 4–NA, 408 nm for 4–NPDA, after transferring Pd@CS/WEO AC hydrogel beads into the respective solutions of 2–NA + $NaBH_4$, 4–NP + $NaBH_4$, 4–NA + $NaBH_4$, and 4–NPDA + $NaBH_4$ (Fig. 5). (Table S1. and Figures S1, S2, S3, S4, S5, S6, S7, S8, S9). The absorption intensities for 2–NA, 4–NP, 4–NA and 4–NPDA remained unchanged for a very long time in the absence of any Pd@CS/WEO AC hydrogel beads, which revealed that the reductions did not proceed without Pd@CS/WEO AC hydrogel beads. As demonstrated in Fig. 5a, the spectrum of 2–NA indicated strong absorption peaks at 414 nm and 284 nm. Upon the addition of Pd@CS/WEO AC hydrogel beads into the $NaBH_4$ + 2–NA solution, the peak intensity at 414 nm dropped with time due to catalytic reduction, and the absorption band for 2–NA shifted from 284 to 293 nm. After 45 s, the peak at 414 nm completely disappeared, confirming that 2–NA was reduced to o–phenylenediamine. The aqueous solution of 4–NP had light yellow color, which gave a peak at 320 nm in accordance with literature data, and it turned bright yellow after the addition of $NaBH_4$, because of its conversion to the 4–nitrophenolate ion (4–NPT). Additionally,

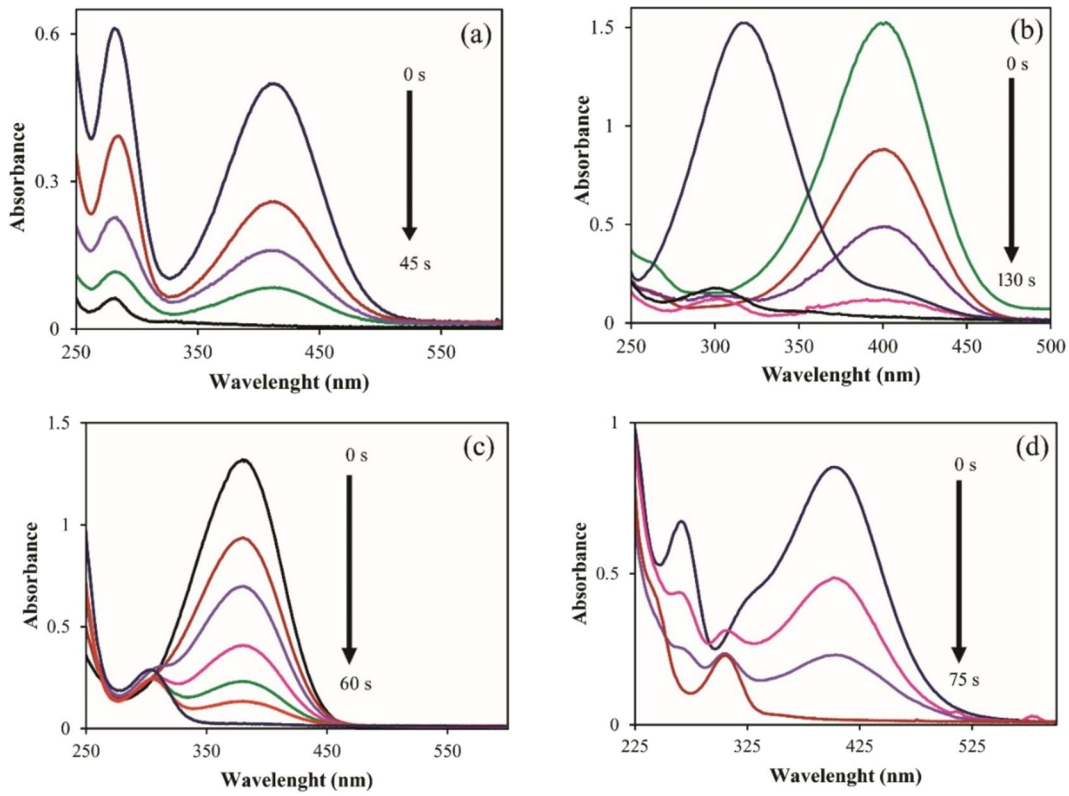

Fig. 5 UV–Vis spectra of 2–NA **a**, 4–NP **b**, 4–NA **c**, and 4–NPDA **d** catalyzed by Pd@CS/WEO AC hydrogel beads

we observed that the peak associated with n—π* transitions of phenolic oxygen at 320 nm shifted to 402 nm, providing further evidence for the formation of 4–NPT (Khalil et al. 2024). When Pd@CS/WEO AC hydrogel beads were introduced into the cuvette, the peak intensity of 4–NPT regularly declined, and the formation of a new peak at 302 nm appeared. The complete reduction of 4–NP has been taken place in 130 s. The progress of 4–NA and 4–NPDA reductions was also monitored by absorbance measurements, and a decline in absorbance at 385 nm and 408 nm for 4–NA and 4–NPDA was observed, respectively. The addition of Pd@CS/WEO AC hydrogel beads into solutions ($4\text{–NA} + NaBH_4$ and $4\text{–NPDA} + NaBH_4$) caused these absorption peaks to gradually disappear, and simultaneously, small shoulder peaks were observed at 307 nm and 309 nm, respectively. As seen in Fig. 5c and d, 4–NA and 4–NPDA were successfully reduced to their corresponding amino compounds (1,4–phenylenediamine and 1,2,4–benzenetriamine) within 1 min and 75 s, respectively. Additionally, we observed that the aqueous solutions of all the studied nitro compounds displayed yellow color, and after reduction, their solutions became colorless.

The kinetic rate constants (k_{app}) were calculated as 0.018 s^{-1}, 0.007 s^{-1}, 0.026 s^{-1}, and 0.012 s^{-1} for 2–NA, 4–NP, 4–NA, and 4–NPDA (Fig. 6), respectively, by using the integral rate law corresponding to first order reactions using following equation:

$$ln\frac{c_t}{c_0} = -kt \tag{2}$$

where c_t and c_0 mean to the concentrations of organic and inorganic contaminants initially and at measured reaction time (t), respectively, and k (s^{-1}) is the rate constant.

Catalytic efficiency of Pd@CS/WEO AC hydrogel beads in reductive degradation of MB, MO, and RhB was also investigated (Table S1). The

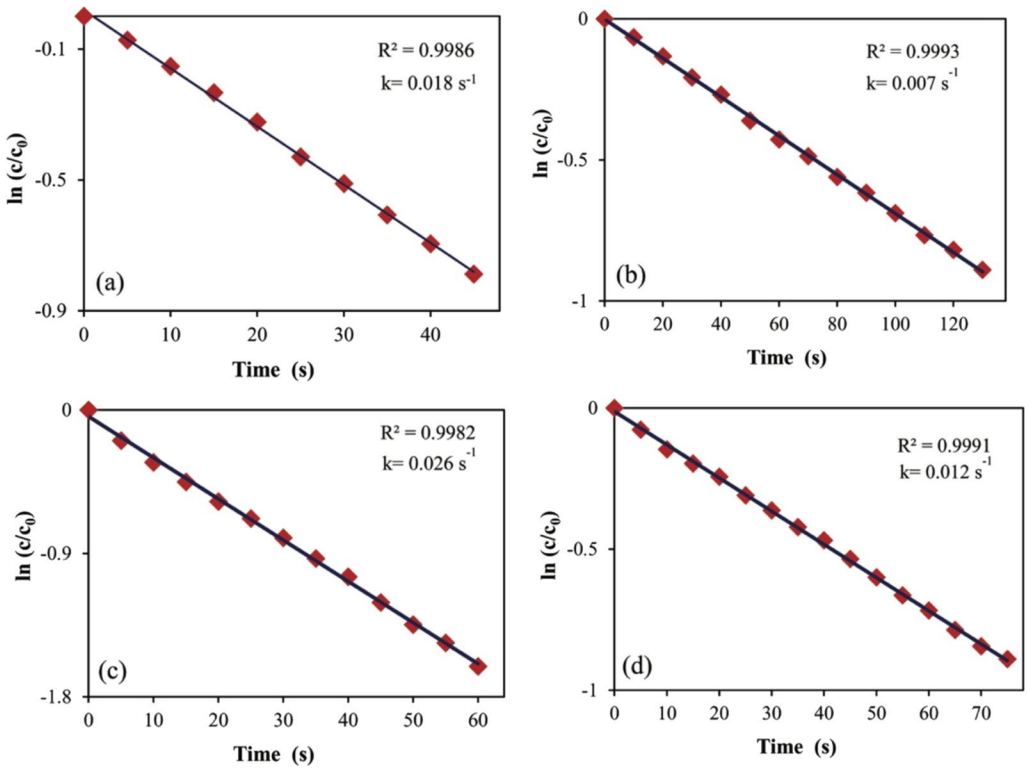

Fig. 6 Rate constants for 2–NA **a**, 4–NP **b**, 4–NA **c**, and 4–NPDA **d** reductions

UV–Vis spectra of MB, MO, and RhB are presented in Fig. 7. The figure shows that MB, MO, and RhB have maximum absorption peaks at 667, 467, and 551 nm, respectively. It was observed that the peak intensities at 667 nm for MB, at 467 nm for MO, and at 551 nm for RhB decreased over time when utilizing Pd@CS/WEO AC hydrogel beads as nanocatalyst together with $NaBH_4$ as reducing agent. After 25 s and 30 s, the MO and RhB dyes were completely degraded by Pd@CS/WEO AC hydrogel beads, and their solutions became colorless during these times. The reductive degradation of MB occurred instantly upon the addition of Pd@CS/WEO AC hydrogel beads to the reaction medium. Additionally, the rate constants for MO and RhB in the presence of Pd@CS/WEO AC hydrogel beads were found as 0.021 s^{-1} and 0.065 s^{-1}, respectively (Fig. 7).

Figure 8 represents proposed degradation mechanism for reduction of rhodamine B into leuco–rhodamne B which is less toxic, and biodegradable compared with RhB (Bhat et al. 2020; Liu et al. 2024b). Initially, hydride transfer takes place from sodium borohydride to Pd–NPs on microbeads followed by adsorption of RhB on microbeads in rate determining step (Step 2). Then, in Step 3, electrons from hydride on NPs were transferred to RhB forming leuco–rhodamine B. Finally, desorption of leuco–rhodamine from surface of catalyst allows Pd@CS/WEO AC hydrogel beads to rejoin the reduction cycle.

In order to validate the applicability of Pd@CS/WEO AC hydrogel beads, we tested its performance in the reduction of $K_3[Fe(CN)_6]$, an inorganic contaminant (Table S1). Aquation solution of $K_3[Fe(CN)_6]$ displayed a strong peak at 418 nm. In the absence of the Pd@CS/WEO AC hydrogel beads, it was determined that no reaction occurred, no color change of solution was observed, and the peak intensity at 418 nm remained unchanged. When the Pd@CS/WEO AC hydrogel beads were added to the reaction solution containing $K_3[Fe(CN)_6] + NaBH_4$, the existing peak at 418 nm began to decrease and disappeared within 30 s. Additionally, the catalytic reduction of $K_3[Fe(CN)_6]$

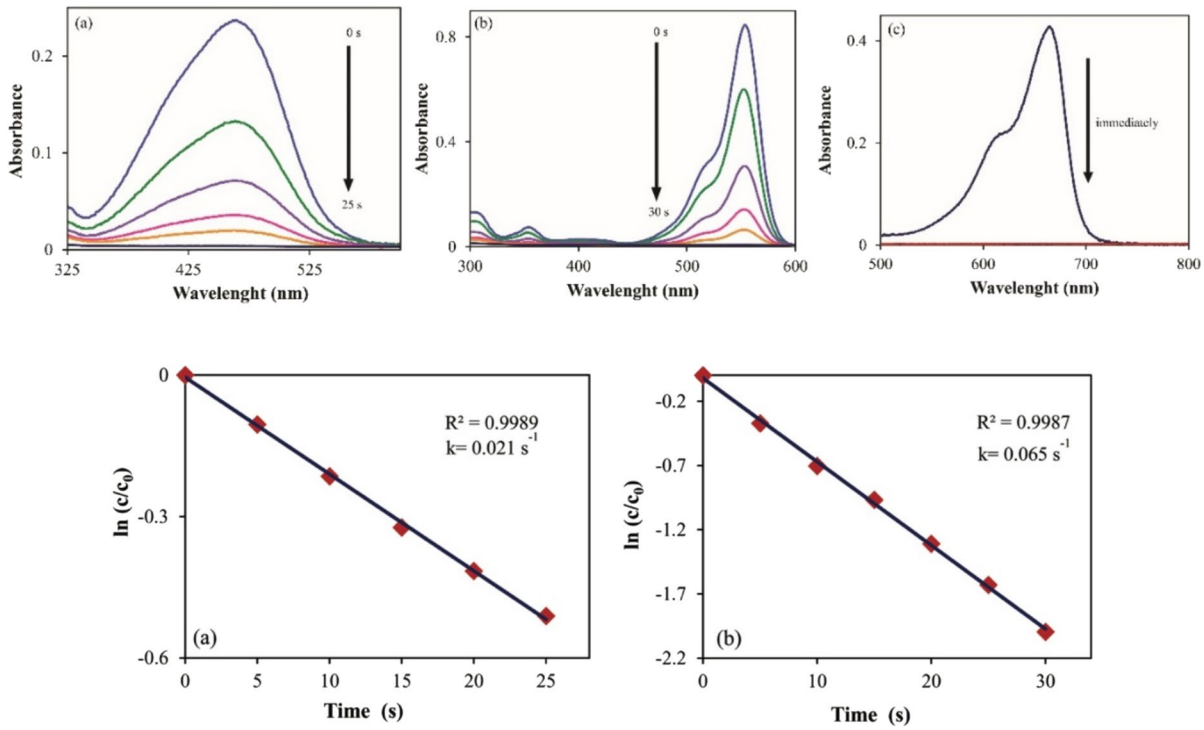

Fig. 7 UV–Vis spectra and rate constant of MO (left), RhB (middle) and MB (right) catalyzed by Pd@CS/WEO AC hydrogel beads

was confirmed with reaction solution became colorless over time. This observation revealed that reduction of $[Fe(CN)_6]^{-3}$ to $[Fe(CN)_6]^{-4}$ was completed out by Pd@CS/WEO AC hydrogel beads in short period of time, and rate constant was calculated as 0.048 s^{-1} (Fig. 9).

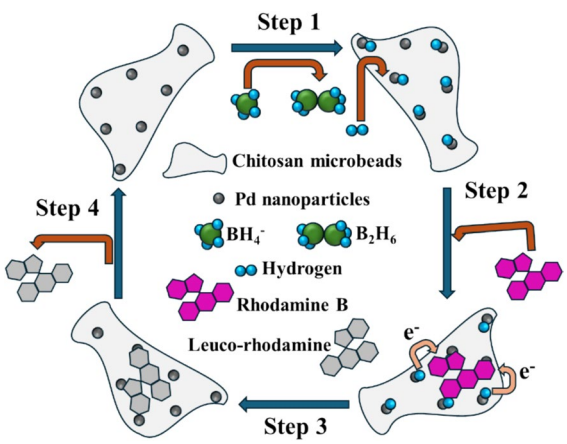

Fig. 8 Proposed reaction mechanism for reduction of RhB

In addition to the reduction of nitroarenes, organic dyes, and $K_3[Fe(CN)_6]$, this part also investigated the efficiency of Pd@CS/WEO AC hydrogel beads in the reduction of Cr(VI) (Table S1). Cr(VI) is considered the most toxic form of chromium. Because Cr(III) is less toxic, as a result, catalytic reduction of Cr(VI) is a current research interest (Becquer et al. 2003). The reduction was easily monitored by UV–Vis analysis. As clearly seen in Fig. 10, the Cr(VI) solution gave a peak at 352 nm. The reduction started immediately after the addition of the 5 mg of Pd@CS/WEO AC hydrogel beads to the $K_2Cr_2O_7$ + HCOOH mixture and the peak intensity at 352 nm decreased over time. The peak intensity completely disappeared within 35 s, accompanied by the yellow solution turning colorless. These observations confirmed the conversion of Cr(VI) to Cr(III) by Pd@CS/WEO AC hydrogel beads. To further confirm the formation of Cr(III), after the reduction of the Cr(VI) reaction was completed, an excess amount of NaOH solution was added to the reaction mixture, and it was observed that the color changed to green. The green color formed after the addition of NaOH indicated

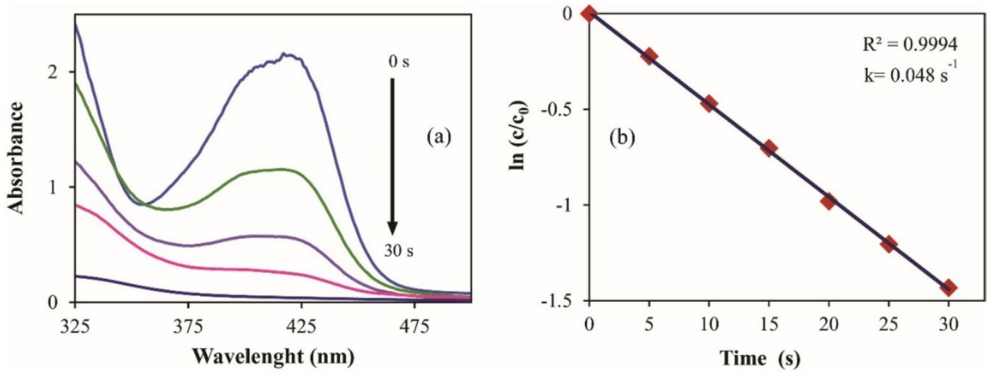

Fig. 9 Catalytic reduction and rate constant of $K_3[Fe(CN)_6]$ catalyzed by Pd@CS/WEO AC hydrogel beads

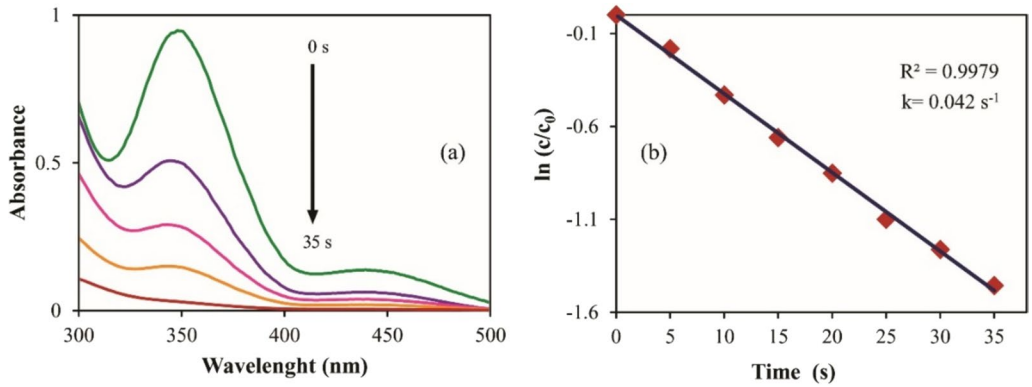

Fig. 10 Catalytic reduction and rate constant of Cr(VI) catalyzed by Pd@CS/WEO AC hydrogel beads

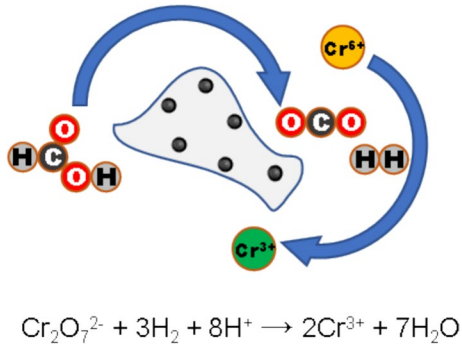

$$Cr_2O_7^{2-} + 3H_2 + 8H^+ \longrightarrow 2Cr^{3+} + 7H_2O$$

Fig. 11 The proposed reduction of Cr(VI) to Cr(III) using Pd@CS/WEO AC hydrogel beads

the formation of chromium(III) hydroxide, confirming the successful reduction of Cr(VI) to Cr(III). Additionally, the rate constant was determined to be 0.042 s^{-1} after the performed kinetic experiments.

As demonstrated in Fig. 11, it is proposed that Cr^{6+} was reduced to Cr^{3+} by Pd@CS/WEO AC hydrogel beads in a two–stage process. In the first stage, formic acid was decomposed into hydrogen and carbon dioxide on the surface of the Pd@CS/WEO AC hydrogel beads after the addition of the catalyst to a mixture of Cr(VI) and formic acid. Then, Cr^{6+} was reduced by the nascent hydrogen generated by the decomposition of HCOOH (Nasrollahzadeh and Issaabadi 2019).

Table 1 summarizes comparison of the performance of Pd@CS/WEO AC hydrogel beads with other catalysts reported in the literature for the reduction of 4–NP, MO, RhB, and MB. The Pd@CS/WEO AC hydrogel beads reported in this study showed better performance compared to other catalysts based on reaction time or rate constant.

Table 1 Comparison of the catalytic power of Pd@CS/WEO AC hydrogel beads with different catalysts for the reduction of 4–NP, MO, RhB, and MB

Pollutant	Catalyst	Time	Rate constant (k)	References
4–NP	Au NPs@C longa	100 s	0.019 s^{-1}	Xie et al. (2024)
	Fe_3O_4@ILD-CoCu	180 s	0.366 min^{-1}	Gholinejad et al. (2024)
	GO-DAP-AgNPs	12 min	7.548×10^{-4} s^{-1}	Nimita Jebaranjitham et al. (2019)
	Pd@CS/WEO AC	130 s	0.007 s^{-1}	present study
MO	0.3Ag/HA	5 (±0.15) min	0.92(±0.045) min^{-1}	Ghosh et al. (2015)
	Ag/TiO_2	9 min	–	Atarod et al. (2016)
	Cu-Ag/GP	4 min	7.67×10^{-3} s^{-1}	Ismail et al. (2018)
	Pd@CS/WEO AC	25 s	0.021 s^{-1}	Present study
RhB	Ag NPs/Thymbra	50 s	8.64×10^{-2} s^{-1}	Veisi et al. (2018)
	S-2 catalyst	14 min	3.73×10^{-1} s^{-1}	Yang et al. (2014)
	$Cu/GO/MnO_2$	4 min	–	Naghdi et al. (2018)
	Pd@CS/WEO AC	30 s	0.065 s^{-1}	Present study
MB	BCDs-Ag/MNPs	60 s	0.0656 s^{-1}	Zahedifar et al. (2020)
	Fe_3O_4@TA/Ag	40 s	0.0685 s^{-1}	Veisi et al. (2019)
	Ni/CPM-1	13 min	0.583 min^{-1}	Veerakumar et al. (2015)
	Pd@CS/WEO AC	immediately	–	Present study

Recyclability of Pd@CS/WEO AC hydrogel beads

High reusability is one of the most significant factors for a catalyst in both academic and industrial applications, besides its high catalytic performance. Thus, reusability and stability of Pd@CS/WEO AC hydrogel beads were investigated in the 4–NP reduction. Due to the nature of Pd@CS/WEO AC hydrogel beads, it was easily recovered from the reaction media by filtering out. Recovered Pd@CS/WEO AC hydrogel beads were washed with water and dried for next runs. Pd@CS/WEO AC hydrogel beads were reused for five successive runs by recovering them at each stage, and it was determined that its performance and structure remained almost the same (Fig. 12).

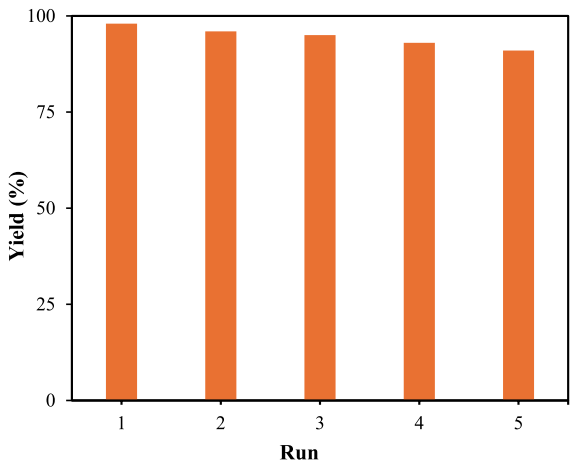

Fig. 12 Reusability of the Pd@CS/WEO AC hydrogel beads for the reduction of 4–NP

Conclusions

Recently, disposal of environmental pollutants is one of the important research areas. In this study, it was aimed to investigate the effect of the Pd@CS/WEO AC catalyst on some environmental pollutants such as aromatic nitro compounds, textile dyes and inorganic oxidants. An activated carbon material was produced from WEO by steam activation and the structure of the material was characterized. The produced activated carbon has 615.4 m^2 g^{-1} surface area and contains predominantly mesopores. The obtained activated carbon was converted into microbeads using chitosan, and a heterogeneous catalyst was produced by doping Pd(0) on the resulting beads. The catalyst Pd@CS/WEO AC was characterized by SEM, TEM, BET, XRD analysis, and the catalytic effeciency of the catalyst was examined in the reduction of various organic and inorganic contaminants, including

nitroarenes (4–NA, 2–NA, 4–NP, 4–NPDA), organic dyes (MB, MO, RhB), Cr(VI), and $K_3[Fe(CN)_6]$. The Pd@CS/WEO AC catalyst reduced nitroarenes in 45–130 s, organic dyes in 0–30 s, $[Fe(CN)_6]^{3-}$ in 30 s, and Cr(VI) in 35 s. The degradation rate constants of catalytic reactions are also higher than similar studies in the literature. Based on kinetic studies, the rate constants for Pd@CS/WEO AC–catalyzed reductions of 2–NA, 4–NP, 4–NA, 4–NPDA, MO, RhB, $[Fe(CN)_6]^{3-}$, and Cr(VI) were found to be 0.018 s^{-1}, 0.007 s^{-1}, 0.026 s^{-1}, 0.012 s^{-1}, 0.021 s^{-1}, 0.065 s^{-1}, 0.048 s^{-1}, and 0.042 s^{-1}, respectively. Moreover, Pd@CS/WEO AC was easily recovered by filtration and reused five times with high catalytic activity. When compared with similar studies in the literature, it was seen that the produced catalyst has high efficiency in terms of both degradation rates and reusability. In addition to its high catalytic activity and reusability, the Pd@CS/WEO AC catalyst is a promising catalytic system for wastewater treatment due to its easy preparation and low cost, along with its environmentally friendly nature.

Author contributions K.K.: made substantial contributions to the conception or design of the work, synthesis activated carbon from waste engine oil N.Y.B.: made investigations for catalytic performance of materials Z.Ö.: made investigation of morphological properties of materials H.T.A.: made investigation of morphological properties of materials T.B.: made contributions to the conception or design of the work.

Funding Open access funding provided by the Scientific and Technological Research Council of Türkiye (TÜBİTAK). The authors declare that no funds, grants, or other support were received during the preparation of this manuscript.

Data availability No datasets were generated or analysed during the current study.

Declarations

Conflict of interests The authors have no relevant financial or non-financial interests to disclose.

Ethical approval Ethics and Consent to Participate declarations: not applicable.

References

Al-Saffar ZH, Yaacob H, Satar MKIM et al (2021) A review on the usage of waste engine oil with aged asphalt as a rejuvenating agent. Mater Today Proc 42:2374–2380. https://doi.org/10.1016/j.matpr.2020.12.330

Arpa O, Yumrutas R, Demirbas A (2010) Production of diesel-like fuel from waste engine oil by pyrolitic distillation. Appl Energy 87:122–127. https://doi.org/10.1016/j.apenergy.2009.05.042

Atarod M, Nasrollahzadeh M, Mohammad Sajadi S (2016) Euphorbia heterophylla leaf extract mediated green synthesis of Ag/TiO_2 nanocomposite and investigation of its excellent catalytic activity for reduction of variety of dyes in water. J Colloid Interface Sci 462:272–279. https://doi.org/10.1016/j.jcis.2015.09.073

Barrett EP, Joyner LG, Halenda PP (1951) The determination of pore volume and area distributions in porous substances. I. computations from nitrogen isotherms. J Am Chem Soc 73:373–380. https://doi.org/10.1021/ja01145a126

Becquer T, Quantin C, Sicot M, Boudot JP (2003) Chromium availability in ultramafic soils from New Caledonia. Sci Total Environ 301:251–261. https://doi.org/10.1016/S0048-9697(02)00298-X

Bhat SA, Rashid N, Rather MA et al (2020) Highly efficient catalytic reductive degradation of rhodamine-B over palladium-reduced graphene oxide nanocomposite. Chem Phys Lett. https://doi.org/10.1016/j.cplett.2020.137724

Brunauer S, Emmett PH, Teller E (1938) Adsorption of gases in multimolecular layers. J Am Chem Soc 60:309–319. https://doi.org/10.1021/ja01269a023

Fedosov SV, Markelov AV, Sokolov AV, Osadchy YuP (2022) Coagulation and ultrafiltration: a hybrid process for purification of used engine oils. Membr Membr Technol 4:297–305. https://doi.org/10.1134/S2517751622050055

Gao Y, Yue Q, Gao B, Li A (2020) Insight into activated carbon from different kinds of chemical activating agents: a

review. Sci Total Environ 746:141094. https://doi.org/10.1016/j.scitotenv.2020.141094

Gholinejad M, Ali Saidiansar M, Eskandari M, Sansano JM (2024) Magnetic nanoparticles supported bimetallic Co-Cu as a catalyst for reductive degradation of hazardous organic compounds in water. Polyhedron 259:117059. https://doi.org/10.1016/j.poly.2024.117059

Ghosh BK, Hazra S, Naik B, Ghosh NN (2015) Preparation of Cu nanoparticle loaded SBA-15 and their excellent catalytic activity in reduction of variety of dyes. Powder Technol 269:371–378. https://doi.org/10.1016/j.powtec.2014.09.027

Hamawand I, Yusaf T, Rafat S (2013) Recycling of waste engine oils using a new washing agent. Energies 6:1023–1049. https://doi.org/10.3390/en6021023

Han R, Li W, Pan W et al (2014) 1D magnetic materials of Fe_3O_4 and Fe with high performance of microwave absorption fabricated by electrospinning method. Sci Rep 4:7493. https://doi.org/10.1038/srep07493

Hao G, Hu Y, Shi L et al (2021) Physicochemical characteristics of chitosan from swimming crab (Portunus trituberculatus) shells prepared by subcritical water pretreatment. Sci Rep 11:1646. https://doi.org/10.1038/s41598-021-81318-0

Hu H, Liu P, Cao S et al (2024) Single metal atoms anchored on N-doped holey graphene as efficient dual-active-component catalysts for nitroarene reduction. Adv Funct Mater. https://doi.org/10.1002/adfm.202307162

Huang J, Li X, Xie R-H et al (2023) Defect anchoring of atomically dispersed Pd on nitrogen-doped holey carbon nanotube for catalytic hydrogenation of nitroarenes. Appl Surf Sci 615:156344. https://doi.org/10.1016/j.apsusc.2023.156344

Ismail M, Khan MI, Khan SB et al (2018) Green synthesis of plant supported Cu Ag and Cu Ni bimetallic nanoparticles in the reduction of nitrophenols and organic dyes for water treatment. J Mol Liq 260:78–91. https://doi.org/10.1016/j.molliq.2018.03.058

Jiménez-Gómez CP, Cecilia JA (2020) Chitosan: a natural biopolymer with a wide and varied range of applications. Molecules 25:3981. https://doi.org/10.3390/molecules25173981

Kaipannan S, Ganesh PA, Manickavasakam K et al (2020) Waste engine oil derived porous carbon/ZnS Nanocomposite as Bi-functional electrocatalyst for supercapacitor and oxygen reduction. J Energy Storage 32:101774. https://doi.org/10.1016/j.est.2020.101774

Kalanidhi K, Nagaraaj P (2022) A green approach for synthesis of highly fluorescent carbon dots from waste engine oil: a strategy for waste to value added products. Diam Relat Mater 121:108724. https://doi.org/10.1016/j.diamond.2021.108724

Khalil A, Khan A, Kamal T et al (2024) Zn/Al layered double hydroxide and carboxymethyl cellulose composite beads as support for the catalytic gold nanoparticles and their applications in the reduction of nitroarenes. Int J Biol Macromol 262:129986. https://doi.org/10.1016/j.ijbiomac.2024.129986

Khan SA, Khan SB, Asiri AM (2016) Toward the design of Zn–Al and Zn–Cr LDH wrapped in activated carbon for the solar assisted de-coloration of organic dyes. RSC Adv 6:83196–83208. https://doi.org/10.1039/C6RA10598J

Lam SS, Liew RK, Cheng CK, Chase HA (2015) Catalytic microwave pyrolysis of waste engine oil using metallic pyrolysis char. Appl Catal B 176–177:601–617. https://doi.org/10.1016/j.apcatb.2015.04.014

Liu D, Fu S, Xu W et al (2024a) Chitosan-functionalized poly(3-hydroxybutyrate) bead as a novel biosupport for palladium in the Suzuki cross-coupling reaction. Colloids Surf A Physicochem Eng Asp 689:133714. https://doi.org/10.1016/j.colsurfa.2024.133714

Liu Z, Kong L, Fei B (2024) Highly efficient catalytic reduction of organic dyes, Cr (VI) and 4-nitrophenol, and photocatalytic degradation of MB by an inorganic–organic hybrid polyoxometalate. Appl Organomet Chem. https://doi.org/10.1002/aoc.7599

Luo X, Jiang L, Zhao R et al (2024) Energy-efficient trehalose-based polyester nanofiltration membranes for zero-discharge textile wastewater treatment. J Hazard Mater 465:133059. https://doi.org/10.1016/j.jhazmat.2023.133059

Maceiras R, Alfonsín V, Morales FJ (2017) Recycling of waste engine oil for diesel production. Waste Manage 60:351–356. https://doi.org/10.1016/j.wasman.2016.08.009

Mopoung S, Dejang N (2021) Activated carbon preparation from eucalyptus wood chips using continuous carbonization–steam activation process in a batch intermittent rotary kiln. Sci Rep 11:13948. https://doi.org/10.1038/s41598-021-93249-x

Naghdi S, Sajjadi M, Nasrollahzadeh M et al (2018) Cuscuta reflexa leaf extract mediated green synthesis of the Cu nanoparticles on graphene oxide/manganese dioxide nanocomposite and its catalytic activity toward reduction of nitroarenes and organic dyes. J Taiwan Inst Chem Eng 86:158–173. https://doi.org/10.1016/j.jtice.2017.12.017

Nasrollahzadeh M, Issaabadi Z (2019) Reduction of Cr(VI) and 4-nitrophenol in aqueous media using N-heterocyclic palladium complex immobilized on the nano Fe_3O_4@SiO_2 as a magnetically recyclable catalyst. Sep Purif Technol 211:809–815. https://doi.org/10.1016/j.seppur.2018.10.045

Neimark AV, Lin Y, Ravikovitch PI, Thommes M (2009) Quenched solid density functional theory and pore size analysis of micro-mesoporous carbons. Carbon N Y 47:1617–1628. https://doi.org/10.1016/j.carbon.2009.01.050

Nimita Jebaranjitham J, Mageshwari C, Saravanan R, Mu N (2019) Fabrication of amine functionalized graphene oxide – AgNPs nanocomposite with improved dispersibility for reduction of 4-nitrophenol. Compos B Eng 171:302–309. https://doi.org/10.1016/j.compositesb.2019.05.018

Ramanathan A, Santhoshkumar A (2019) Feasibility analysis of pyrolysis waste engine oil in CRDI diesel engine. Energy Proc 158:755–760. https://doi.org/10.1016/j.egypro.2019.01.201

Sargin I (2019) Efficiency of Ag(0)@chitosan gel beads in catalytic reduction of nitroaromatic compounds by sodium borohydride. Int J Biol Macromol 137:576–582. https://doi.org/10.1016/j.ijbiomac.2019.07.018

Scherrer P (1918) Nachrichten von der Gesellschaft der Wissenschaften zu Göttingen, Mathematisch-Physikalische Klasse. Mathematisch-Physikalische Klasse 98–100

United Nation (UN-Water) (2021) Summary Progress Update 2021 : SDG 6 — water and sanitation for all. UN-Water integrated monitoring initiative 1–58

Suriani AB, Alfarisa S, Mohamed A et al (2015) Quasi-aligned carbon nanotubes synthesised from waste engine oil. Mater Lett 139:220–223. https://doi.org/10.1016/j.matlet.2014.10.046

Taya N, Agarwal J (2024) Unmodified 'chitosan in water' as an efficient and recyclable heterogeneous catalytic system for the synthesis of bis(indolyl)methanes. Appl Catal A Gen 670:119539. https://doi.org/10.1016/j.apcata.2023.119539

Thommes M, Kaneko K, Neimark AV et al (2015) Physisorption of gases, with special reference to the evaluation of surface area and pore size distribution (IUPAC Technical Report). Pure Appl Chem 87:1051–1069. https://doi.org/10.1515/pac-2014-1117

Tkaczyk A, Mitrowska K, Posyniak A (2020) Synthetic organic dyes as contaminants of the aquatic environment and their implications for ecosystems: a review. Sci Total Environ 717:137222. https://doi.org/10.1016/j.scitotenv.2020.137222

Ullah A, Tekbaş M, Doğan M (2023) The impact of economic growth natural resources urbanization and biocapacity on the ecological footprint: the case of Turkey. Sustainability. https://doi.org/10.3390/su151712855

Veerakumar P, Chen S-M, Madhu R et al (2015) Nickel nanoparticle-decorated porous carbons for highly active catalytic reduction of organic dyes and sensitive detection of Hg(II) Ions. ACS Appl Mater Interfaces 7:24810–24821. https://doi.org/10.1021/acsami.5b07900

Veisi H, Azizi S, Mohammadi P (2018) Green synthesis of the silver nanoparticles mediated by Thymbra spicata extract and its application as a heterogeneous and recyclable nanocatalyst for catalytic reduction of a variety of dyes in water. J Clean Prod 170:1536–1543. https://doi.org/10.1016/j.jclepro.2017.09.265

Veisi H, Moradi SB, Saljooqi A, Safarimehr P (2019) Silver nanoparticle-decorated on tannic acid-modified magnetite nanoparticles (Fe_3O_4@TA/Ag) for highly active catalytic reduction of 4-nitrophenol, Rhodamine B and Methylene blue. Mater Sci Eng, C 100:445–452. https://doi.org/10.1016/j.msec.2019.03.036

Wang M, Yu Q (2017) Pore structure characterization of carboniferous shales from the eastern Qaidam Basin, China: combining helium expansion with low-pressure adsorption and mercury intrusion. J Pet Sci Eng 152:91–103. https://doi.org/10.1016/j.petrol.2017.02.007

Widodo S, Khoiruddin K, Ariono D et al (2020) Re-refining of waste engine oil using ultrafiltration membrane. J Environ Chem Eng 8:103789. https://doi.org/10.1016/j.jece.2020.103789

Wyckoff RWG (1963) Crystal structures 1, 2nd edn. Interscience Publishers, New York, New York

Xie W, Zhang Y, Yang X et al (2024) Green synthesis of gold nanoparticles mediated by extract of Curcuma longa under ultrasonic condition: investigation of its application for reduction of dye pollutants and repairing the articular cartilage in an animal model of osteoarthritis of the knee. Inorg Chem Commun 162:112169. https://doi.org/10.1016/j.inoche.2024.112169

Yang X, Zhong H, Zhu Y et al (2014) Highly efficient reusable catalyst based on silicon nanowire arrays decorated with copper nanoparticles. J Mater Chem A Mater 2:9040. https://doi.org/10.1039/c4ta00119b

Zahedifar M, Seyedi N, Salajeghe M, Shafiei S (2020) Nanomagnetic biochar dots coated silver NPs (BCDs-Ag/MNPs): a highly efficient catalyst for reduction of organic dyes. Mater Chem Phys 246:122789. https://doi.org/10.1016/j.matchemphys.2020.122789

Zhao R, Li Y, Mao Y et al (2022) Recycling the high-salinity textile wastewater by quercetin-based nanofiltration membranes with minimal water and energy consumption. Environ Sci Technol 56:17998–18007. https://doi.org/10.1021/acs.est.2c06397

Zhao J, Zhang A, Li Y et al (2024) Pd nanoparticles decorated N-doped holey graphene assembled on aluminum silicate fibers agglomerate for catalytic continuous-flow reduction of nitroarenes. Chem Eng Sci 286:119656. https://doi.org/10.1016/j.ces.2023.119656

Zheng X, Zhao J, Xu M, Zeng M (2020) Preparation of porous chitosan/reduced graphene oxide microspheres supported Pd nanoparticles catalysts for Heck coupling reactions. Carbohydr Polym 230:115583. https://doi.org/10.1016/j.carbpol.2019.115583